Design of integrated hybrid silicon waveguide optical gyroscope

Sudharsanan Srinivasan,* Renan Moreira, Daniel Blumenthal and John E. Bowers

Department of Electrical and Computer Engineering, University of California, Santa Barbara, CA 93106, USA
sudhas@ece.ucsb.edu

Abstract: We propose and analyze a novel highly integrated optical gyroscope using low loss silicon nitride waveguides. By integrating the active optical components on chip, we show the possibility of reaching a detection limit on the order of 19°/hr/√Hz in an area smaller than 10 cm^2. This study examines a number of parameters, including the dependence of sensitivity on sensor area.

OCIS codes: (060.2800) Gyroscopes; (230.7370) Waveguides; (120.5790) Sagnac effect.

References and links

1. Merlo, M. Norgia, and S. Donati, *Handbook of Fibre Optic Sensing Technology* (John Wiley & Sons, 2000), Chap. 16.
2. M. J. R. Heck, J. F. Bauters, M. L. Davenport, J. K. Doylend, S. Jain, G. Kurczveil, S. Srinivasan, Y. Tang, and J. E. Bowers, "Hybrid silicon photonic integrated circuit technology," IEEE J. Sel. Top. Quant. **19**, 6100117 (2013).
3. J. F. Bauters, M. L. Davenport, M. J. R. Heck, J. K. Doylend, A. Chen, A. W. Fang, and J. E. Bowers, "Silicon on ultra-low-loss waveguide photonic integration platform," Opt. Express **21**(1), 544–555 (2013).
4. M. Piels, J. F. Bauters, M. L. Davenport, M. J. R. Heck, and J. E. Bowers, "Low-loss silicon nitride AWG demultiplexer heterogeneously integrated with hybrid III–V/silicon photodetectors," J. Lightwave Technol. **32**(4), 817–823 (2014).
5. R. A. Bergh, H. C. Lefevre, and H. J. Shaw, "An overview of fiber-optic gyroscopes," J. Lightwave Technol. **2**(2), 91–107 (1984).
6. J. F. Bauters, M. J. R. Heck, D. Dai, J. S. Barton, D. J. Blumenthal, and J. E. Bowers, "Ultralow-loss planar Si3N4 waveguide polarizers," IEEE Photon. J. **5**(1), 6600207 (2013).
7. A. DeGroote, "A broadband LED on the hybrid silicon platform using multiple die bonding and quantum well intermixing," M. S. thesis, University of California, Santa Barbara, CA, 2013.
8. R. Moreira, J. Barton, M. Belt, T. Huffman, and D. Blumenthal, "Optical Interconnect for 3D Integration of Ultra-Low Loss Planar Lightwave Circuits," in Advanced Photonics 2013, H. Chang, V. Tolstikhin, T. Krauss, and M. Watts, eds., OSA Technical Digest (online) (Optical Society of America, 2013), paper IT2A.4.
9. J. M. Mackintosh and B. Culshaw, "Analysis and observation of coupling ratio dependence of Rayleigh backscattering noise in a fiber optic gyroscope," J. Lightwave Technol. **7**(9), 1323–1328 (1989).
10. K. H. Wanser, "Fundamental phase noise limit in optical fibres due to temperature fluctuations," Electron. Lett. **28**(1), 53–54 (1992).

1. Introduction

Low cost and compact gyroscopes are very useful in the fields of radar, robotics, aeronautics, automotives and gaming [1]. An optical gyroscope based on the Sagnac effect is a versatile technique to measure angular rotation. Unlike mechanical gyroscopes, which rely on conservation of angular momentum, optical gyroscopes have no moving parts and are not affected by gravity, shock or vibrations. This implies that optical gyroscopes require less maintenance and do not require any special gimbal mounting or packaging. The development of low-loss single-mode optical fibers for the telecommunication industry allowed for its use in an all-fiber optical gyroscope (FOG). These are now commonly used in tactical grade systems. Although FOGs do not require any active path length control, the sensitivity depends on the length of the fiber coil and is a major limitation to its size.

#212027 - $15.00 USD Received 13 May 2014; revised 2 Aug 2014; accepted 8 Aug 2014; published 7 Oct 2014

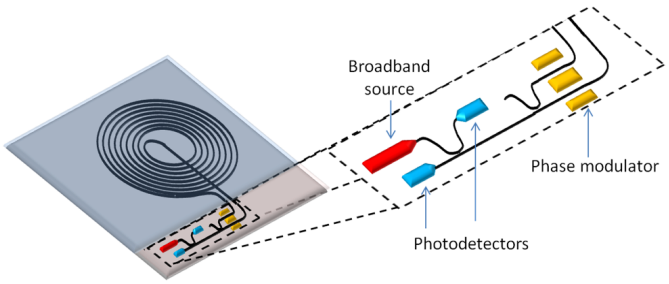

Fig. 1. Schematic of the photonic chip in a gyroscope using monolithic waveguides (solid black lines) and integrated photonic devices.

We propose a design for a new fully integrated optical gyroscope that can reach a detection limit of 19°/hr/√Hz. This design allows for wafer-scale manufacturing and hence lowers the cost of an individual sensor. More importantly the packaging cost, which is the largest fraction of the total cost in all FOG and micro-electromechanical system (MEMS) based sensors, can be significantly lower with this technology. The operating principle is identical to the FOG where two counter-propagating light signals experience different phase shifts proportional to the rotation rate. The desired signal is measured by interfering these signals on a photodetector and recording the photocurrent. By replacing each component with its counterpart on-chip, we can realize a photonic circuit that is suitable for rotation sensing. A schematic of the photonic circuit integrated on a common silicon substrate is shown in Fig. 1.

A silicon substrate has two main advantages for the integration of all the active and passive elements. First, the use of silicon substrates enables large scale, robust and inexpensive manufacturing of active optical devices, viz. lasers, modulators and detectors, on a single chip using the hybrid silicon platform [2]. The capability to integrate with complementary metal-oxide-semiconductor (CMOS) electronic devices allows for compact packaging and lower noise from interference. Second, by integrating low propagation loss silicon nitride waveguides [3], several meters of delay can be achieved which increases the sensitivity of the sensor, as described below. To achieve low loss, high temperature deposition and annealing are necessary, which requires silicon or glass substrates. The integration of silicon nitride waveguides with active optical devices was shown to be possible in [4], where hybrid silicon photodetectors were integrated with a silicon nitride arrayed waveguide grating (AWG) to fabricate an eight channel receiver. The following discussion is divided into three sections: device design, results and conclusions. We will extensively study the various aspects of this sensor and provide a design methodology to achieve the best sensitivity.

2. Device design

The circuit in Fig. 1 is used in rotation sensing because it is reciprocal, and hence robust to vibration, temperature variations, coupler variations and other imperfections [5]. Optical fiber can support two polarization modes, and hence polarization rotation is an issue in FOGs. On the other hand, the silicon nitride waveguides described in [3] are highly birefringent and can be designed to allow only the transverse-electric (TE) mode to propagate with low loss [6].

The use of a broadband source is necessary to minimize the effects of scattering and reflections. The reflections within the source coherence length from the loop center have to be minimized as they can add in phase with the primary light beams and show up as spurious rotation signal. The coherence length of superluminescent diodes (SLD) can be in the range of a few tens of micrometers and SLDs are commonly used to improve sensitivity. Hybrid III-V silicon SLEDs with 293nm of gain bandwidth have been demonstrated [7]. The use of monolithic planar waveguides forces the need for waveguide crossings in order to have a net non-zero Sagnac phase shift. Each waveguide crossing is a site for reflections and

#212027 - $15.00 USD Received 13 May 2014; revised 2 Aug 2014; accepted 8 Aug 2014; published 7 Oct 2014

transmission loss. Additionally, the primary light beams see each crossing twice in a single round trip. By spacing the waveguide crossings a coherence length away, the reflected light only adds in intensity and not phase.

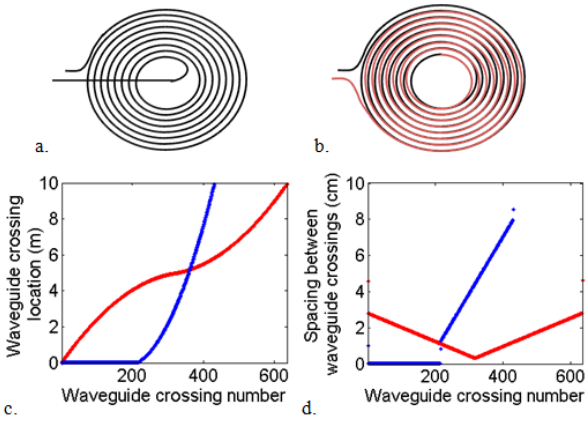

Fig. 2. Top view of (a) single layer and (b) double layer spiral waveguide. The waveguide in the second layer is colored red for clarity. (c) Waveguide crossing locations and (d) spacing between crossings, as a function of waveguide crossing number, as seen by a counterclockwise propagating beam in Fig. 2a. The total length and center-to-center waveguide spacing are 10m and 50μm respectively. Blue dots and red dots correspond to single layer and double layer Si_3N_4 waveguide platforms respectively. The disruption in the blue curve in Fig. 2d occurs when the light beam has encountered all the crossings once, on the way into the spiral.

Figure 2 shows the spiral waveguide designs for a single layer and a double layer topology [8]. The latter allows for stacking spirals one above the other to reduce the footprint. The coupling between the layers is achieved by means of an adiabatic vertical directional coupler. The coupling loss for each transition between layers has been measured to be 0.2dB [8], however, the reflections need to be quantified. The location of waveguide crossings and the spacing between them, for the two topologies, as encountered by the counter-clockwise propagating light beam is shown in Figs. 2(c) and 2(d) respectively. The total length is 10m and we consider an Archimedean spiral structure with center-to-center waveguide spacing of 50μm and a minimum waveguide bend radius of 1mm. The waveguide crossings in the single layer design are at 90° and those in the double layer design are very acute. In both topologies, we observe that the crossings can be designed to be hundreds to thousands of coherence lengths away from the center of the loop. Another source of reflection is the transition from the silicon nitride waveguide to the silicon waveguide. The location of these transitions can be offset from the coupler by greater than a coherence length. Coupling losses of (0.4 ± 0.2)dB per transition with a 20nm 3dB bandwidth and losses of (0.8 ± 0.2)dB per transition with a 100nm 3dB bandwidth for two different taper designs have been reported [3].

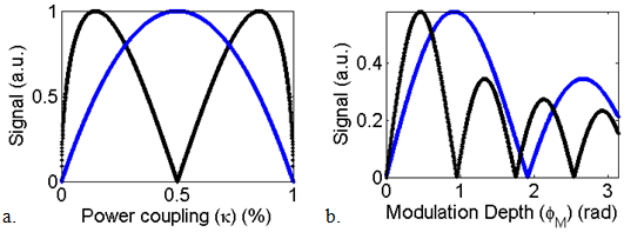

Fig. 3. Sagnac signal (blue) and backscatter signal (black) as a function of (a) coupling ratio, and (b) modulation depth on the phase modulator.

The next design aspect is the coupler ratio. The effect of a non-ideal 50/50 coupler can increase the fraction of backscatter signal in the measured signal. Using the approach described in [9] for a push-pull phase modulator, we plot the dependence of backscatter noise

#212027 - $15.00 USD Received 13 May 2014; revised 2 Aug 2014; accepted 8 Aug 2014; published 7 Oct 2014

with coupling ratio and modulation depth. Figure 3(a) shows the need for a precise 50/50 coupler to suppress the back scatter signal. The use of a tunable coupler allows for correcting process variations at a wafer scale. Figure 3(b) shows that the modulation depth near the first maximum in the Sagnac signal is also when the backscatter signal is minimized.

3. Results

The expression for photocurrent at the detector as a function of the phase shift between the two counter-propagating beams can be derived to be

$$I = \frac{\eta P_0}{8} e^{-\alpha L}\left(1+\cos\left(\frac{\pi}{2}+\Delta\theta\right)\right) \tag{1}$$

where η is a conversion factor in A/W which includes the responsivity of the detector and other fixed losses excluding the couplers, P_0 is the optical power from the source, α is the waveguide loss, L is the length of the sensor and Δθ is the non-reciprocal phase shift. The argument of the cosine term has a π/2 term to bias at maximum sensitivity. This can be achieved using a silicon phase modulator. An additional phase tuner can be added for closed loop linear operation. We assume this mode of operation to evaluate fundamental limits of this approach.

With this as the starting point we derive expressions for the root-mean-squared (RMS) noise in the measured phase shift ($\Delta\phi_{net}$) due to various noise sources and calculate the smallest detectable rotation using the following relations.

$$\Omega_{\text{minimum}} = \frac{\Delta\phi_{net}}{\partial(\Delta\theta)/\partial\Omega} \tag{2}$$

$$\Delta\theta = \frac{8\pi A}{c\lambda_0}\Omega \tag{3}$$

where Ω is the angular rotation rate, c is the speed of light, λ_0 is the mean wavelength of light, A is the total enclosed area of the Sagnac loop.

We consider four sources of noise, viz. thermal noise of the preamplifier, shot noise, relative intensity noise of the source and thermo-refractive noise. The expression for each phase noise term and the net phase noise from all contributions can be written as

$$\Delta\phi_{RIN} = \sqrt{10^{RIN/10}}\, rad/\sqrt{Hz} \tag{4}$$

$$\Delta\phi_{thermal} = \frac{10^{-9}}{\eta P_0 e^{-\alpha L}\sqrt{R}}\, rad/\sqrt{Hz} \tag{5}$$

$$\Delta\phi_{shot} = \frac{1.6\times10^{-9}}{\sqrt{\eta P_0 e^{-\alpha L}}}\, rad/\sqrt{Hz} \tag{6}$$

$$\Delta\phi_{thermo-refractive} = 4.3\times10^{-7}\sqrt{\frac{L}{40}}\, rad/\sqrt{Hz} \tag{7}$$

$$\Delta\phi_{net} = \Delta\phi_{RIN} + \Delta\phi_{thermal} + \Delta\phi_{shot} + \Delta\phi_{thermo-refractive} \tag{8}$$

where RIN is the relative intensity noise of the source in dBc/Hz, R is the termination resistance for the detector, assumed to be 1kohm, and L is the length in meters. The value for thermo-refractive noise is obtained from [10].

#212027 - $15.00 USD Received 13 May 2014; revised 2 Aug 2014; accepted 8 Aug 2014; published 7 Oct 2014

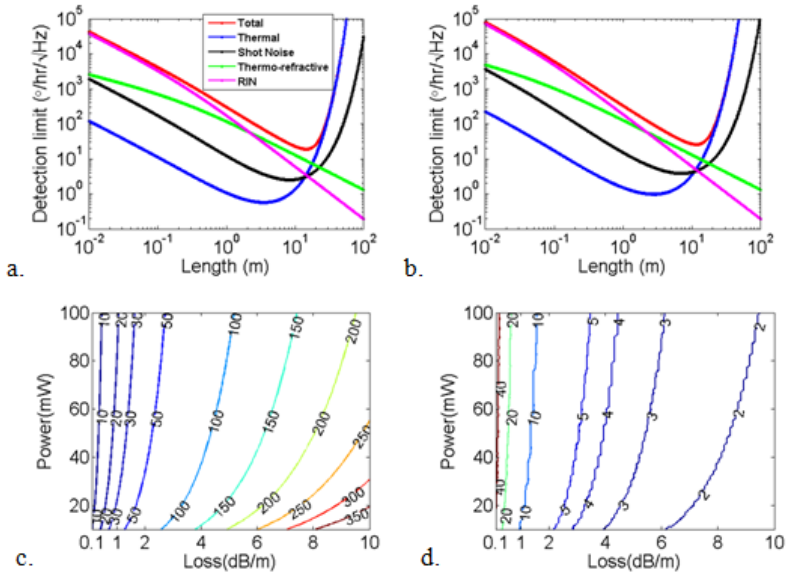

Fig. 4. Contributions from various noise sources to the rotation noise spectral density as a function of Sagnac loop length for P_0 = 100mW and loss = 1dB/m; (a) single layer (b) double layer. Contours of minimum measurable rotation (c), in °/hr/√Hz, and optimum loop length to obtain that sensitivity (d), in meters, as a function of source power and waveguide loss for single layer topology.

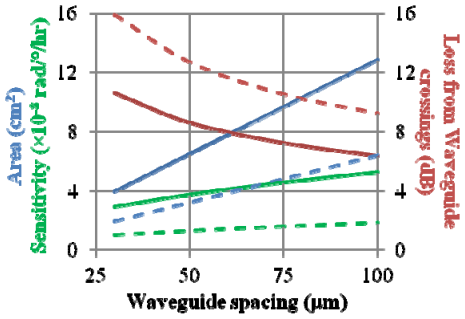

Fig. 5. Chip area (blue), rotation sensitivity (green) and loss from waveguide crossings (red) as a function of waveguide spacing, for a 10m long, 3μm wide waveguide, as used for ultralow loss 100nm thick Si_3N_4 waveguide core. The solid lines and dashed lines correspond to single layer and double layer Si_3N_4 waveguide platforms, respectively.

Figures 4(a) and 4(b) show the contribution from each noise term to the rotation noise spectral density for a given source power and waveguide loss, for a single and double layer topology respectively. The minimum from the two plots are 19°/hr/√Hz and 25.6°/hr/√Hz respectively. However, the area of the chip for the two cases is 9.2cm^2 and 3.7cm^2 respectively. These results indicate that the use of a double layer topology is very powerful in reducing the chip area for only a small degradation in sensitivity. However, the tradeoff between coupling efficiency between layers and waveguide crossing loss for different spacer thicknesses will ultimately decide the benefit of this design. Figures 4(c) and 4(d) show the minimum measurable rotation and the optimum loop length to obtain that sensitivity, as a function of source power and waveguide loss for a single layer. The assumed value for RIN is −140dBc/Hz. The waveguide crossing loss has been measured to be 0.02dB/crossing and included in the calculation by incorporating it into the value of η. To reduce waveguide crossing losses, one could transition to a second layer of nitride waveguides. From Fig. 4(a)

#212027 - $15.00 USD Received 13 May 2014; revised 2 Aug 2014; accepted 8 Aug 2014; published 7 Oct 2014

we see that RIN is a dominant source of noise for short loop lengths and the detection limit is ultimately limited by the thermo-refractive noise for longer lengths. The modulation frequencies, applied to the phase modulators, for loop lengths above 2m is less than 50MHz.

Figure 5 shows the chip area, rotation sensitivity and loss from waveguide crossings as a function of waveguide center-to-center spacing, for a 10m long and 3μm wide waveguide, as used for ultralow loss 100nm thick Si_3N_4 waveguide core. In order to reduce the chip area, the spacing needs to be small. However, the number of waveguide crossings to achieve 10m waveguide length also increases, increasing the round-trip loss. The gradual increment in sensitivity comes from the increasing outer loop diameter. We also note that the spacing has a lower limit from the source coherence length. The double layer design helps to bring down the area by a factor of two. However, the waveguide crossing loss, assuming a loss value of 0.02dB/crossing, is high because of the increased number of crossings for the same length. The sensitivity is lower due to the reduced outer loop diameter.

4. Conclusions

We propose and analyze a novel rotation sensor using the hybrid silicon platform, which allows for integration of all the required active and passive optical elements on a chip. The sensor area using a ten meter long waveguide and 50μm waveguide spacing is smaller than $6.5cm^2$ for a single layer of Si_3N_4 waveguide. We derive expressions for RMS noise in detected phase shift signal from various noise sources and compared their respective contributions to the minimum detectable rotation rate. By integrating a broadband source and optimally designing the low loss waveguide loop the impairments due to scattering and reflections can be minimized, to reach detection limits down to 19°/hr/√Hz for a loss of 1 dB/m and 4.2°/hr/√Hz for a loss of 0.1 dB/m, using a single layer topology.

Acknowledgment

We would like to thank Ralph Bergh, Robert Lutwak, Daryl T. Spencer and Jared Bauters for useful discussions and comments. This research was supported by DARPA MTO.

#212027 - $15.00 USD Received 13 May 2014; revised 2 Aug 2014; accepted 8 Aug 2014; published 7 Oct 2014